Title: Photoluminescence of Ce3+ and Eu2+ in low-P ternesite from the Negev Desert, Israel

Author: Maria Czaja, Marta Stasiak, Zbigniew Mazurak

Citation style: Czaja Maria, Stasiak Marta, Mazurak Zbigniew. (2017). Photoluminescence of Ce3+ and Eu2+ in low-P ternesite from the Negev Desert, Israel. "Physics and Chemistry of Minerals" (Vol. 44, Iss. 8, s. 553-559), doi, 10.1007/s00269-017-0882-5

CrossMark

ORIGINAL PAPER

Photoluminescence of Ce³⁺ and Eu²⁺ in low-P ternesite from the Negev Desert, Israel

Maria Czaja[1] · Marta Stasiak[1] · Zbigniew Mazurak[2]

Abstract For the first time, the photoluminescence of ions of Ce³⁺ and Eu²⁺ in natural low-P ternesite has been measured. The emission bands of Ce³⁺ ions at 405, 426, and 440 nm and the corresponding excitation wavelengths suggest the presence of Ce³⁺ ions in three different cationic sites. In the photoluminescence spectra of Eu²⁺, emission bands at 530 and 620 nm can be seen that originate from two different cationic sites. In addition, it is demonstrated that an energy transfer occurs between Ce³⁺ and Eu²⁺ ions situated in those cationic sites where the force of the crystallic field is weakest. The photoluminescence spectra were obtained for a thin section sample with low contents of these two elements (41.2 ppm Ce, 2.11 ppm Eu).

Keywords Photoluminescence · Ce³⁺ · Eu²⁺ · Ternesite · Larnite–ye'elimite rock

Introduction

Among the spectroscopic properties of rare-earth ions, it is observed that ions with $4f^n$ to $4f^n-^15d^1$ transitions involve the promotion of a single electron from the 4 f orbital to an empty 5d orbital. These transitions which are parity allowed (Laporte's selection rule is obeyed) result in high oscillator strengths and are strongly affected by the host

✉ Maria Czaja
maria.czaja@us.edu.pl

1 Faculty of Earth Sciences, University of Silesia, Będzińska 60, 41-200 Sosnowiec, Poland

2 Centre of Polymer and Carbon Materials, Polish Academy of Sciences, Marie Curie-Skłodowskiej 34, 41-819 Zabrze, Poland

lattice as the 5d electron is the outer. The absorption and luminescence spectra of Eu²⁺ and Ce³⁺ consist of the 5d-4f broadbands ranging from ultraviolet to visible light. The schemes of ground and excited energy levels of Ce³⁺ and Eu²⁺ are presented in Fig. 1. The excited 5d levels split into 2 or 5 components depending on the crystal-site symmetry, usually by 18,000 cm⁻¹. The ground level of Ce³⁺ splits into two components, $^2F_{7/2}$ and $^2F_{5/2}$, due to spin–orbit coupling (2000 cm⁻¹). In general, Ce³⁺ shows doublet emission bands due to this ground state coupling level. However, the separation of the emission bands into two bands is not clearly visible and can by shown only using Gaussian curve fitting. The emission of Ce³⁺ and Eu²⁺ originates from the lowest crystal-field components of the 5d state to ground state levels. These energy of emission bands depend on crystal fields splitting in each particular host lattice and, if the crystal-field parameter 10 Dq is large, the emission shifts towards longer wavelengths. The magnitude of d-orbital splitting of a metal center is given by the following equation:

$$Dq = \frac{Z^* \cdot e^2 \cdot r^4}{6 \cdot R^5} \qquad (1)$$

where Z^* is the valence of anion ligand, e is the electron charge, r is the radius of the frontier, and R is the distance between metal center and ligand. vanUitret (1984) proposed the empirical formula (Eq. 2) for the positions of the emission bands of Ce³⁺ and Eu²⁺:

$$E\,(\text{cm}^{-1}) = Q\left\{1 - \left(\frac{V}{4}\right)^{\frac{1}{V}} \cdot 10^{-\Phi}\right\} \qquad (2)$$
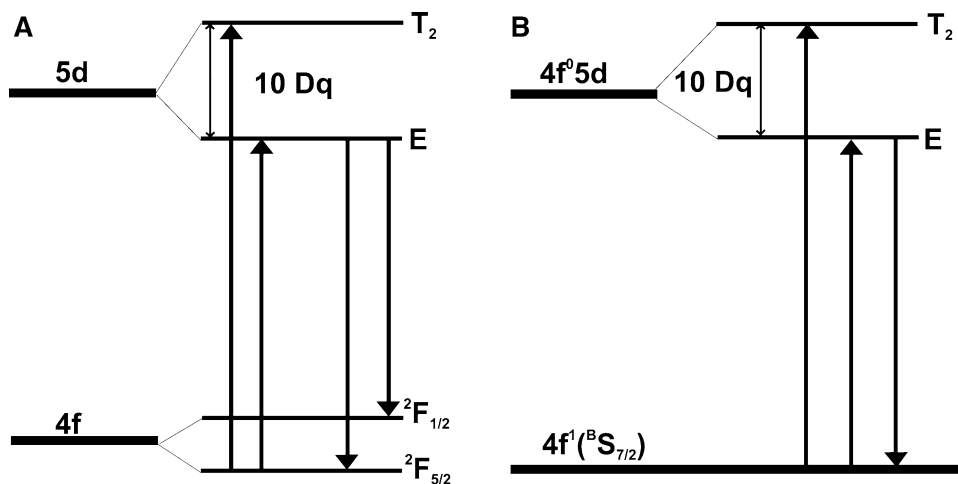
where $\Phi = \frac{n \cdot E_a \cdot r}{80}$ and $E\,(\text{cm}^{-1})$ is the position of the Ce³⁺ or Eu²⁺ emission band, Q is the position of the energy of the lower d-band edge, namely, $Q = 50{,}000$ and $34{,}000$ cm⁻¹

Fig. 1 Simplified diagram of ground and excited levels of **a** Ce^{3+} and **b** Eu^{2+} for coordination number CN = 8 without point of symmetry; 10 Dq is crystal-field splitting parameter, T_2 and E – triplet and doublet excited levels

for Ce^{3+} and Eu^{2+}, respectively, and V is the valence of activator ions (3 or 2 for cerium or europium, respectively), n is the number of anions in the immediate shell around the impurity ion, Ea is the electron affinity of the atoms that form the anions, and r is the radius of the main host cation replaced by Ce^{3+} or Eu^{2+}. As the positions of emission bands are directly proportional to the product of n and r, this formula allows the prediction the positions of the emission bands of an ion in different host materials in which only one kind of anion exists (Geng et al. 2013; Zhang et al. 2011).

In ternesite, and in silicocarnotite, there are three different non-equivalent cationic sites which have quite diverse lengths of Ca-O bonds and diverse effective charges on oxygen ions (Gałuskin et al. 2016). For the purposes of this research of low-P ternesite, it was necessary to establish the strength of crystal-field splitting, which must take into account not only the diverse Ca-O lengths, but also different values of the effective charges on each ith oxygen in various coordination polyhedrons around Ca^{2+}. The following formulas (3) are proposed:

$$\frac{q_{Ce} \cdot q_i}{6 \cdot R_i^5}, \quad \frac{q_{Eu} \cdot q_i}{6 \cdot R_i^5} \tag{3}$$

where q_{Ce}, q_{Eu} is the cation charge, q_i is the ligand effective charge, and R_i the distance between the cation (Ce^{3+} or Eu^{2+}) and the ith oxygen. This charge is different for oxygen atoms in different tetrahedra; the charge is −1 for SiO_4, −0.75 for PO_4, and −0.5 for SO_4.

Most of the measured Ce^{3+} and Eu^{2+} luminescence spectra for the minerals studied show broad emission bands, i.e., single or double bands in the 320–390 nm range for Ce^{3+} and in the 395–450 nm range for Eu^{2+} ions (Gaft et al. 2005; Gorobets and Rogonije 2002, http://www.fluomin. org/uk). To date, the photoluminescence spectra of lanthanide ions in natural ternesite, silicocarnotite, or ellestadite ($Ca_5(SiO_4,PO_4,SO_4)_3(F,OH,Cl)$) have not been measured.

However, the spectra of 4fion emission in synthetic silicocarnotite $Ca_5[SiO_4(PO_4)](PO_4)$ have been obtained. Geng et al. (2013) have done so for Ce^{3+}, Tb^{3+}, and Mn^{2+}. The emission band of Ce^{3+} is asymmetric with a maximum wavelength of 416 nm. Geng et al. (2013) have proposed to fit this band into four Gauss components, namely, 380, 405, 439 and 483 nm originating from three non-equivalent cationic sites. The emission band had been measured only for one excitation wavelength: λ_{exc} = 305 nm. It was proposed (Geng et al. 2013) that for Ce^{3+} ions occupying cationic sites with greater Ca-O distances, the emission occurs at shorter wavelengths. It was concluded that the first two emission bands at 380 and 405 nm originate from the Ca(1) site and those at 439 and 483 nm from the Ca(2) and Ca(3) sites, respectively. In addition, the phenomenon of the $Ce^{3+} \rightarrow Tb^{3+}$ and $Ce^{3+} \rightarrow Mn^{2+}$ energy transfer has been demonstrated. For synthetic silicocarnotite $Ca_5[SiO_4(PO_4)](PO_4)$ doped with 0.03 apfu Eu^{2+} (Yu et al. 2013), the broad emission band at 425–625 nm was measured and divided into three components at 485, 527, and 579 nm. These were ascribed to three different Ca^{2+} cationic sites in the lattice of this compound which contain Eu^{2+}. The component at 485 nm showed the greatest intensity; measurement of the emission band for that component yielded a value of λ_{exc} = 365 nm. The excitation spectra for the other components of the emission bands were not sought. The parameters of the elementary cell of this compound correspond to JCPDS file no. 73-1181 data and similar to those for natural silicocarnotite from the Hatrurim Comlex (Gałuskin et al. 2016). Another synthetic substance, composed of $Ca_5[SiO_4(PO_4)](PO_4)$ doped with Eu^{2+} ions, and with cationic parameters corresponding to JCPDS file no 40-09393 (Roh et al. 2012), exhibited a broad emission band for the 0.05 apfu Eu concentration. When the band was divided into three Gaussian components, the most intensive was that at 509 nm followed by those at 561 and 621 nm. In this case, only the excitation

wavelength at 290 nm was measured. The differences of the Eu^{2+} ion emission bands' values in both substances reflect the differences in coordination numbers and in Eu–O distances (Roh et al. 2012; Yu et al. 2013).

Roh et al. (2012) and Yu et al. (2013) concluded that the asymmetric shape of the emission bands of Ce^{3+} and Eu^{2+} ions built into the synthetic silicocarnotite resulted from the presence of these ions in three different cationic sites. Because of the differences in Ca–O distances for each of the cationic sites, this is likely. However, these authors ignored the fact that for Ce^{3+} ion spectra, emission components with energy differences of <2000 cm^{-1} can serve as emission transitions from the same center to the $^2F_{7/2}$ and $^2F_{5/2}$ sublevels. In addition, in their papers, the emission band component with the greatest wavelength had the lowest intensity and the greatest full width at half maximum (FWHM). This component may be the result of strong coupling between the 5d electrons of Ce^{3+} or Eu^{2+} and lattice vibrations. In this case, many phonons can be involved in the optical transitions and emission band becomes very wide. This kind of reservation may also be expressed regarding the Ce^{3+}-derived emission component at 483 nm (Geng et al. 2013) and Eu^{2+}-derived emission components at 621 nm (Roh et al. 2012) and at 579 nm (Yu et al. 2013). It is most prevalent frequent for those emission centers and host materials for which the Stokes shift, i.e., the difference in energies of excitation and emission bands is large. The Stokes shift according to data given by Geng et al. (2013) for ions of Ce^{3+} in silicocarnotite is 12,190 cm^{-1}. For Eu^{2+} emission, the Stokes shift is 15,735 cm^{-1} (Roh et al. 2012) or 7195 cm^{-1} (Yu et al. 2013). Substantial lattice deformations in the 5d excited state give rise to large Stokes shifts.

Defining the excitation of the bands related to different excitation wavelengths would provide irrefutable evidence that the emission bands of a given ion originate from different cationic sites. This, however, was not done in Roh et al. (2012) and Yu et al. (2013).

Experimental

Fluorescence steady-time measurements were performed using a Jobin–Yvon (SPEX) spectrofluorimeter FLUOR-LOG 3–12 at room temperature using a 450 W xenon lamp, a double-grating monochromator, and a Hamamatsu 928 photomultiplier. The wavelength range for emission and excitation spectra was from 250 to 900 nm, and the resolution was no greater than 1 nm. We set ourselves the task of verifying whether it is possible to perform correctly the luminescence measurements of minerals in the form of small grains from the petrographic thin section. The initial investigation was based on the following steps:

Fluorescence measurement is typically performed at a right angle (90°) from transmitted or scattered light. However, the reflected light can interfere with accurate data collection. Therefore, samples in the form of pellets, powdered at monolayers on microscope slides, are mounted at 22.5 degrees to the incident beam. The thin section was then set for 22.5 degrees to incident beam. The beam's dimension was 25 mm × 3 mm.

The primary excitation wavelength for Ce^{3+} was λ_{exc}=290 nm, according to our earlier studies (Czaja et al. 2013). We subsequently verified that the recorded spectrum was correct, i.e., that we did not measure reflections from xenon lamp nor Raman shift.

Using the option of real-time measurements' setting, we searched for the specimen setting in which the intensity of emission wavelength was the greatest. We moved the specimen surface relative to the incident beam very carefully, so that the maximum possible number of of ternesite grains was covered by incident beam.
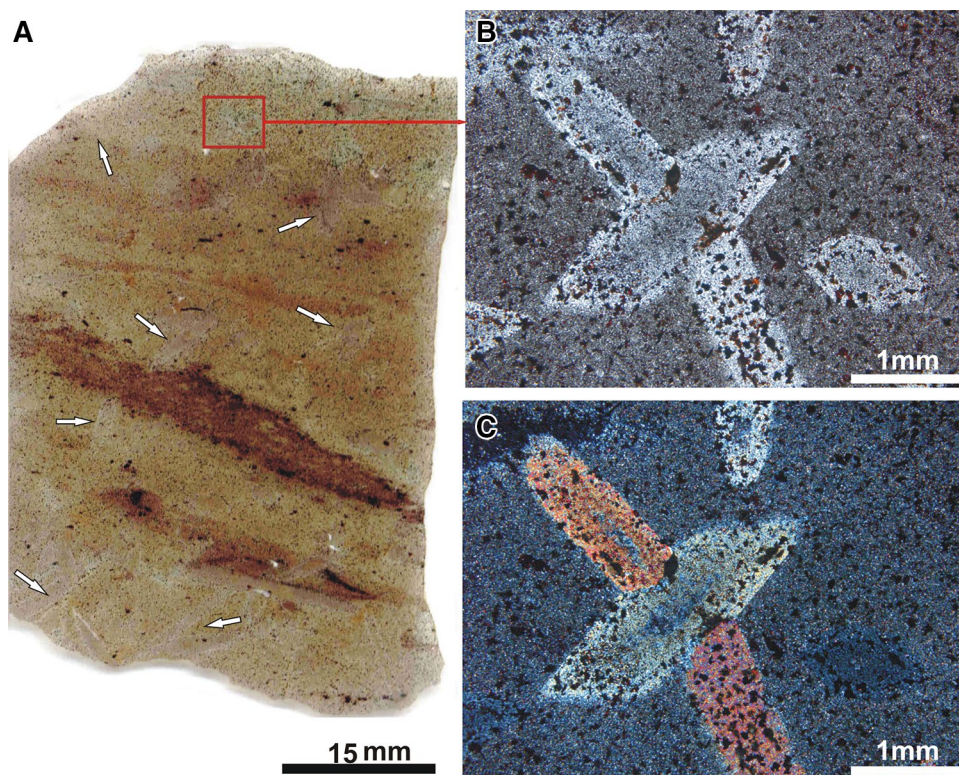
After these initial steps, the measurements were carried out just as for monocrystal samples; and it was the connection of the emission band with the excitation line which caused this emission. It has thus been established that the studied ternesite grains have only exhibited the luminescence of of Ce^{3+} and Eu^{2+} ions.

The thin section sample was that of a fine-grained larnite–ye'elimite rock containing metacrysts (>20 mm) of ternesite. The columnar grains of theses minerals are shown in Fig. 2. In earlier work [Gałuskin et al. 2016], it was noted that in CL, only ternesite grain exhibited luminescence. The studied P-low ternesite contained 41.2 ppm Ce, 2.11 ppm Eu (Vapnik et al. 2015). However, the intensive photoluminescence spectra for this sample have been successively measured.

Results and discussion

According to the chemical- and X-ray analysis presented in Gałuskin et al. (2016), the low-P ternesite has the formula $Ca_5[(Si_{0.9}P_{0.1})O_4]_2[(S_{0.8}P_{0.2})O_4]$. This means that the tetraedric position T1 is occupied mostly by S, while the T2 site is occupied by Si. In low-P ternesite, as in silicocarnotite, the existence of three non-equivalent cationic sites has been determined for Ca cations. The coordination number for the Ca(1), Ca(2), and Ca(3) sites in ternesite is 7, as it is for Ca(2) and Ca(3) in silicocarnotite though, in this compound, it is 8 for Ca(1). For natural silicocarnotite, the mean lengths of the Ca-O bonds are Ca(1)=2.537 Å, Ca(2)=2.454 Å, and Ca(3)=2.415 Å (Gałuskin et al. 2016), while, for the synthetic compound, they are 2.5455, 2.4646, and 2.4211 Å, respectively (Geng et al. 2013). For low-P ternesite, the mean bond lengths are Ca(1) =

Fig. 2 Thin section (**a**) of pyrometamorphic rock from the Negev Desert, Israel. *White arrows* indicate ternesite crystals observed under petrographic microscope (**b** parallel nicols, **c** crossed nicols)

2.482 Å, Ca(2) = 2.496 Å, and Ca(3) = 2.432 Å. As in silicocarnotite, the shortest Ca–O distances are for the Ca(3) cationic site, and the greatest for the Ca(2) site. For the latter, one significantly greater length has been established; Ca(2)-O$_3$ = 3.0586 Å, with the others in the 2.32–2.56 Å range. We have calculated the mean quadratic elongation of Ca–O distances as follows:

$$\langle l_7 \rangle = \frac{1}{7} \sum_{i=1}^{7} \left[\frac{l_i - \bar{l}}{\bar{l}} \right]^2 \tag{4}$$

where l_7 [Å] is the mean quadratic elongation for coordination number CN = 7, l_i are the current i Ca–O distances, and $\bar{l}$ is the mean Ca-O distance for the given Ca site. These values are 1.30, 0.04, and 0.02 for the Ca(2), Ca(1), and Ca(3) sites, respectively.

The greater the negative charge on oxygen and the shorter the length of the cation-ligand bond, the greater the energy difference between the excited state and the basic state. When the energy difference grows, the energy of the radiation being emitted decreases. This means that the greater the energy difference, the longer the corresponding emission wavelength. For the various Ca sites in silicocarnotite and ternesite, we have calculated, based on data from Gałuskin et al. (2016), the magnitude of d-orbital splitting for Ce^{3+} and Eu^{2+} using the formulas at (3). For the Ce^{3+} ions in silicocarnotite, they are Ca(1) = 1032 × 10^{-4}, Ca(2) = 1000 × 10^{-4},

Ca(3) = 1110 × 10^{-4} and, for Eu^{2+}, Ca(1) = 688 × 10^{-4}, Ca(2) = 667 × 10^{-4}, and Ca(3) = 740 × 10^{-4}. These values can differ for Ce^{3+}, although the differences between the Ca(1) and Ca(2) sites are not significant. One may expect two or three luminescence centers—three emission bands originating from Ce^{3+} ions. The shortest emission band should be related to the Ca(2) site, whereas the longest should originate from the Ca(3) site. However, Geng et al. (2013), taking only the influence of the Ca-O distance on the emission transition energy into account, suggested that the shortest emission wavelength originates from Ca(1) and the longest from Ca(3). For Eu^{2+}, the difference of the calculated magnitudes of d-orbital splitting is not so significant. One can, therefore, conclude that Eu^{2+} ions in Ca(1) and Ca(2) sites can exhibit the same emission wavelengths. For Ce^{3+} ions in low-P ternesite, the magnitudes of d-orbital splitting are Ca(1) = 1100 × 10^{-4}, Ca(2) = 990 × 10^{-4}, and Ca(3) = 1200 × 10^{-4} whereas, for Eu^{2+}, they are Ca(1) = 735 × 10^{-4}, Ca(2) = 660 × 10^{-4}, Ca(3) = 800 × 10^{-4}. In our calculations, we have taken into account not only different Ca–O bond lengths and different oxygen charges related to T1 and T2 tetrahedrons, but also the fact that these tetrahedrons are occupied as follows: T1—0.8 S and 0.2 P; tetrahedron T2—0.9 Si and 0.1 P. For ternesite, the orbital splitting parameters for the various cationic sites clearly differ from one another. One can, therefore, expect three different emission bands where the shortest emission

wavelength corresponds to the Ca(2) sites and the longest wavelength to Ca(3).

In line with the expectations, for the studied sample of grains of low-P ternesite, emissions from Ce^{3+} ions situated in three different cationic sites were measured. The emission at 405 nm is excited by the 275 nm line and originates from cerium ions in the Ca(2) site, while the emission at 426 nm, excited by the 288 nm line, originates from the Ca(1) site. Finally, the emission at 440 nm, excited by the 305 nm line, is related to the Ca(3) site (Fig. 3). The emission bands are asymmetrical, as seen in Fig. 4. The decomposition of the emission band for the $\lambda_{exc} = 275$ nm, with the maximum at 405 nm, results in two Gaussian components with maximum thresholds at 407 nm and 440 nm. They are separated by an energy difference of 1843 cm^{-1}, similar to the value of the splitting of the ground level ^{2}F. It can, therefore, be concluded that the emission bands at 407 and 440 nm represent emission to sublevels $^2F_{5/2}$ and $^2F_{7/2}$, respectively. The ratio of the integral intensivies of these components is 5:1, corresponding to the frequent observations that emission to the $^2F_{7/2}$ sublevel is less intensive than that to the $^2F_{5/2}$ sublevel (Senden and Meijerink 2016). The measured emission and excitation spectra reveal that the excitation band at 305 nm only causes the emission observed at 440 nm, without provoking those observed at 405 or 426 nm. The intensity of these three emission bands presented in Fig. 3 has not been changed. The intensities of those at 405 and 440 nm are nearly identical, although the power of the excitation source, the xenon lamp, is almost twice as low for $\lambda_{exc} = 275$ nm than for $\lambda_{exc} = 305$ nm. The intensity of the emission at 426 nm is smaller than at the other two wavelengths. This means that the occupation of

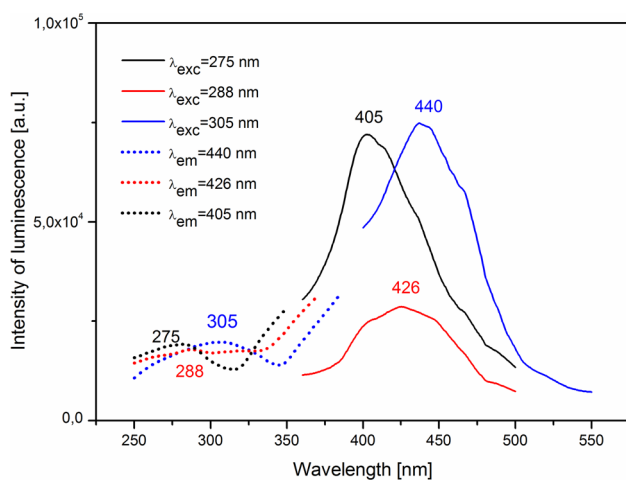**Fig. 4** Emission band of Ce^{3+} divided into two Gaussian components

cationic sites by cerium ions is the smallest in the Ca(1) site.

As shown in Fig. 5, the energy of emission bands (the strength of crystal-field splitting) depends not only on the mean ion-ligand distance (blue point in Fig. 5), but also on the effective charges of each ith oxygen in various coordination polyhedrons around Ca^{2+} (black point in the Fig. 5). The Pearson correlation coefficient for the data obtained using our formula (3) was $\rho = -0.99$, 398, and for the B $\rho = -0.89$, 443.

The Stokes shift for Ca(2) is the greatest at 11,673 cm^{-1}, less significant for Ca (1) at 11,248 cm^{-1}, and least of all for Ca(3) at 10,060 cm^{-1}. It merits noting that the values of the mean quadratic elongation for the Ca sites follow the same order.

For Eu^{2+}, emissions at 530 and 620 nm (Fig. 5) are confirmed as originating from two different cationic sites by the different excitation bands of these two emission lines.

Fig. 3 Photoluminescence spectra of Ce^{3+} in low-P ternesite. *Solid lines* emission spectra, *dotted lines* excitation spectra, Ca(2) site *black lines*, Ca(1) *red lines*, Ca(3) *blue lines*
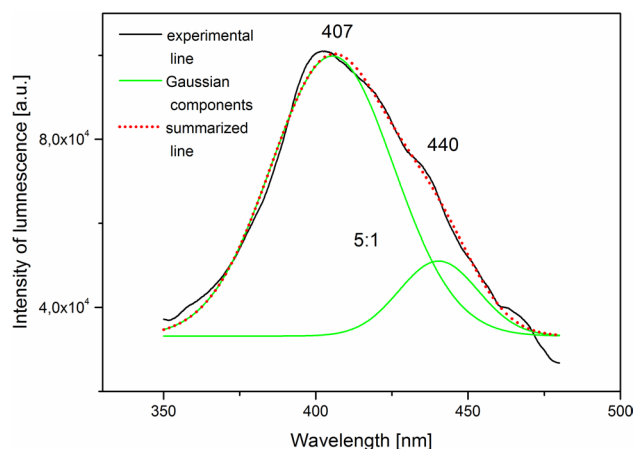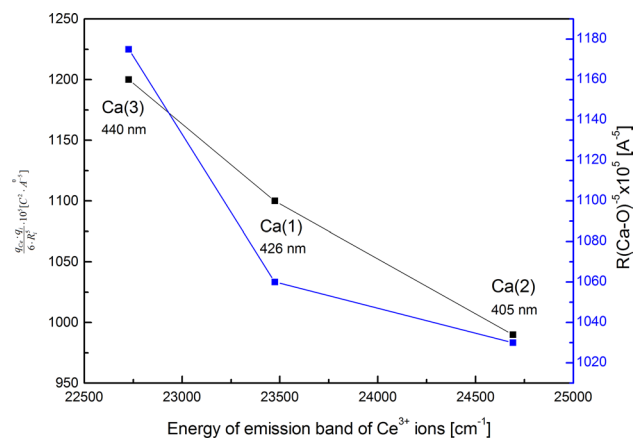

Fig. 5 Dependence of Ce^{3+} emission bands on the Ca-O distance and on the effective charge of ligands

The emission at 530 nm can be attributed to europium ions in positions of a weak crystallic field—Ca(2) and Ca(1)—while the position at 620 nm can be attributed to ions situated in site Ca(3). It has been observed that the emission at 530 nm is excited by both the 399 nm and the 407 bands, that is, by emissions originating from Ce^{3+} ions. This effect should be interpreted as the result of the transfer of energy from Ce^{3+} to Eu^{2+}, as depicted in Fig. 6. The intensity of emission at the 530 nm band is more than three times that at the 620 nm wavelength. The difference is probably due not only to the effect of the $Ce^{3+} \rightarrow Eu^{2+}$ energy transfer (Fig. 7), but also to the heterogenous occupation of the cationic sites. It is certainly not due to aperture, because the excitation power of the xenon lamp for $\lambda_{exc} = 399$ nm or 407 nm is less than that at $\lambda_{exc} = 480$ nm by a ratio of 3:4. In addition, it bears underlining that the luminescence intensity of Eu^{2+} ions is half that of Ce^{3+} ions with the obvious explanation being the greater cerium content compared to europium.

The emission bands of Ce^{3+} and Eu^{2+} ions in the studied ternesite have wavelengths greater than those measured thus far for many other minerals, e.g., agrellite, calcite, danburite, feldspar, fluorite, fluorapatite, leucophanite, or plagioclase. In other synthetic compounds, e.g., $CaAl_2O_4$ i $SrAl_2O_4$ (Zhang et al. 2011; Massera et al. 2015; Ueda et al. 2015), Sr_3SiO_5 (Sun et al. 2008), $SiO_2-Al_2O_3-CaO$ (Nishiura and Tanabe 2008), $SiO_2-Al_2O_3-CaO-CaF_2$ (Fu et al. 2009), Cs_2SO_4, K_2SO_4 and Rb_2SO_4 (Kishan Kumar et al. 1991), $KMgSO_4Cl$ and $Na_5(PO_4)SO_4$ (Gedam et al. 2008), $2SrO-nB_2O_3-(1-n)P_2O_5$ (Wang et al. 2008), $M_2Si_5N_8$ (M=Ca, Sr, Ba) (Li et al. 2006), and $CaSrAl_2SiO_7$ (Miao et al. 2015), Ce^{3+} emission bands usually have a wavelength of 390–450 nm, whereas, for Eu^{2+} emission bands, wavelengths are of 470–570 nm. Clearly, the sort of material in which these ions are incorporated determines the character of their emissions.

Summary

1. It has been demonstrated that the three measured emission bands of Ce^{3+} ions originate from three nonequivalent cationic sites. The occupation of these sites is not uniform; site Ca(2) is occupied by the greatest number of cerium ions.
2. The emissions from Eu^{2+} are represented by two bands. It is likely that the more intensive band at 530 nm is related to two cationic sites.
3. An energy transfer occurs among the Ce^{3+} and Eu^{2+} ions occupying the Ca(2) sites where the splitting of the crystallic field is smallest.
4. The wavelengths of the emission bands of Ce^{3+} and Eu^{2+} in low-P ternesite and in synthetic silicocarnotite crystals are similar. For Ce^{3+}, these are the 407 and 440 nm bands and, for Eu^{2+}, the 530 and 620 nm bands.
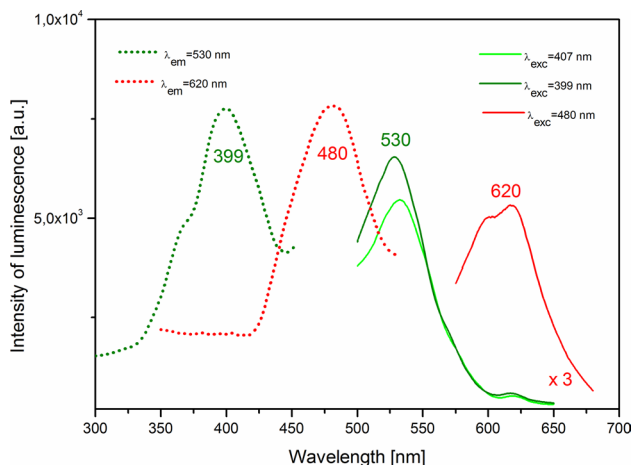

Fig. 6 Photoluminescence spectra of Eu^{2+} in low-P ternesite. *Solid lines* emission spectra, *dotted lines* excitation spectra, *green lines* probable Ca(2) and Ca(1) sites, *red lines* Ca(3) site
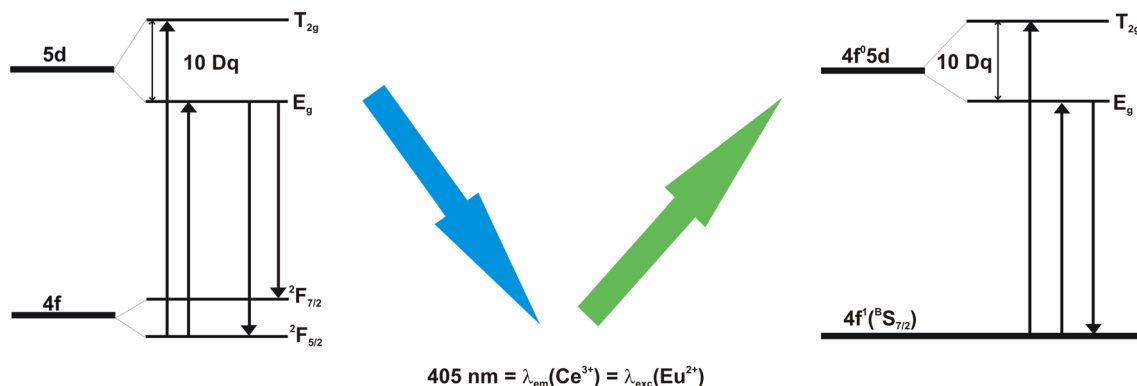

Fig. 7 Simplified diagram of $Ce^{3+} \rightarrow Eu^{2+}$ energy transfer

5. It is proposed that the magnitude of d-orbital splitting be estimated in accordance with a formula (formula 3 above) which takes into account not only diverse cation–anion distances but also differences between effective charges of ligands in different coordination polyhedrons.

6. In certain cases, it is possible to carry out luminescence measurements from minerals in the form of small grains from the petrographic thin section, even without the confocal microscopic device.

References

Czaja M, Bodył-Gajowska S, Mazurak Z (2013) Steady-state luminescence measurements for qualitative identification of rare earth ions in minerals. JMPS 108:47–54

Fu J, Kobayashi M, Sugimoto S, Parker JM (2009) Scintillation from Eu^{2+} in Nanocrystallized Glass. J Am Ceram Soc 92:2119–2121

Gaft M, Reisfeld R, Panczer G (2005) Luminescence spectroscopy of minerals and materials. Springer-Verlag, Berlin

Gałuskin EV, Gałuskina IO, Gfeller F, Kruger B, Kusz J, Vapnik Y, Dulski M, Dzierżanowski P (2016) Silicocarnotite, $Ca_5[(SiO_4)(PO_4)](PO_4)$, a new "old" mineral from the Negev Desert, Israel, and the ternesite-silicocarnotite solid solution: indicators of high-temperature alteration of pyrometamorphic rocks of the Hatrurim Complex, Southern Levant. Eur J Mineral 28:105–123

Gedam SC, Dhoble SJ, Moharil SV (2008) Eu^{2+} and Ce^{3+} emission in sulphate based phosphors. J Lum 128:1–6

Geng D, Shang M, Zhang Y, Lian H, Cheng Z, Lin J (2013) Tunable luminescence and energy transfer properties of $Ca_5(PO_4)_2SiO_4:Ce^{3+}/Tb^{3+}/Mn^{2+}$ phosphors. J Mater Chem 1:2345–2353

Gorobets BS, Rogonije AA (2002) Luminescence spectra of minerals. All-Russia Institute of Mineral Resources (VIMS), Moscow

Kishan Kumar VS, Acharyulu BSVSR, Sastry SBS (1991) Eu^{2+} luminescence in alkali sulphate lattice. J Mater Sci 26:1069–1072

Li YQ, de With G, Hintzen HT (2006) Luminescence properties of Ce^{3+}-activated alkaline earth silicon nitride $M_2Si_5N_8$ (M = Ca, Sr, Ba). J Lum 116:107–116

Massera J, Gaussiran M, Gluchowski P, Lastusaari M, Hupa L, Petit L (2015) Processing and characterization of phospate glasses containing $CaAl_2O_4:Eu^{2+}$, Nd^{3+} and $SrAl_2O_4:Eu^{2+}$, Dy^{3+} microparticles. J Eur Ceram Soc 35:3863–3871

Miao S, Xia Z, Molokeev MS, Zhang J, Liu Q (2015) Crystal structure refinement and luminescence properties of blue-green-emitting $CaSrAl_2SiO_7:Ce^{3+}$, Li^+, Eu^{2+} phosphors. J Mater Chem C 3:8322–8328

Nishiura S, Tanabe S (2008) Preparation and optical properties of Eu^{2+} and Sm^{3+}-co-doped glass ceramic phosphors emitting white color by violet laser excitation. J Ceram Soc Jpn 116:1096–1099

Roh H-S, Hur S, Song HJ, Park IJ, Yim DK, Kim D-W, Hong KS (2012) Luminescence properties of $Ca_5(PO_4)_2SiO_4:Eu^{2+}$ green phosphors for near UV-based white LED. Mater Lett 70:37–39

Senden T, Meirejink A (2016) The d-f luminescence of Eu^{2+}, Ce^{3+} and Yb^{2+} ions in $Cs_2MP_2O_7$ (M = Ca^{2+}, Sr^{2+}). J Lum 177:254–260

Sun X, Zhang J, Zhang X, Luo Y, Wang X-J (2008) Long lasting yellow phosphorescence and photosimulated luminescence in $Sr_3SiO_5:Eu^{2+}$ and $Sr_3SiO_5:Eu^{2+}$, Dy^{3+} phosphors. J Phys D: Appl Phys 41:195414–195417. doi:10.1088/0022-3727/41/19/195414

Ueda J, Shinoda T, Tanabe S (2015) Evidence of three different Eu^{2+} sites and their luminescence quenching processes in $CaAl_2O_4$:Eu. Opt Mater 41:84–89

vanUitert LG (1984) An empirical relation fitting the position in energy of the lower d-band edge for Eu^{2+} or Ce^{3+} in various compounds. J Lum 29:1–9

Vapnik Y, Gałuskina I, Palchik V, Sokol EV, Gałuskin E, Lindsley-Griffin N, Stracher GB (2015) Stone-Tool Workshops of the Hatrurim Basin, Israel: mineralogy, geochemistry and rock mechanics of lithic industrial materials. In: Stracher GB, Prakash A, Sokol EV (eds) Coal and peat fires: a global perspective, 3. Elsevier, Amsterdam, pp 281–316. doi:10.1016/B978-0-444-59509-6.00010-7

Wang F, Song H, Pan G, Fan L, Dong B, Liu L, Bai X, Qin R, Ren X, Zheng Z, Lu S (2008) Luminescence properties of Ce^{3+} and Tb^{3+} ions codoped strontium borate phosphate phosphors. J Lum 128:2013–2018

Yu H, Deng D, Li Y, Xu S, Li Y, Yu C, Ding Y, Lu H, Yin H, Nie Q (2013) Electronic structure and luminescence properties of $Ca_5(PO_4)_2SiO_4:Eu^{2+}$ green emitting phosphor for white emitting diodes. Opt Commun 289:103–108

Zhang J, Zhang X, Shi J, Gong M (2011) Luminescence properties of green- or red- emitting Eu^{2+} -doped $Sr_3Al_2O_6$ for LED. J Lum 131:2463–2467